AFRL-RV-PS-
TR-2019-0009

OPTICAL SPECTROSCOPY OF INFRARED DETECTOR MATERIALS UNDER HYDROSTATIC PRESSURE

Stefan Zollner

New Mexico State University
Office of Sponsored Programs
1050 Stewart St., Ste E1200
Las Cruces, NM 88003

1 April 2019

Final Report

AIR FORCE RESEARCH LABORATORY
Space Vehicles Directorate
3550 Aberdeen Ave SE
AIR FORCE MATERIEL COMMAND
KIRTLAND AIR FORCE BASE, NM 87117-5776

DTIC COPY

NOTICE AND SIGNATURE PAGE

Using Government drawings, specifications, or other data included in this document for any purpose other than Government procurement does not in any way obligate the U.S. Government. The fact that the Government formulated or supplied the drawings, specifications, or other data does not license the holder or any other person or corporation; or convey any rights or permission to manufacture, use, or sell any patented invention that may relate to them.

This report is the result of contracted fundamental research which is exempt from public affairs security and policy review in accordance with AFI 61-201, paragraph 2.3.5.1. This report is available to the general public, including foreign nationals. Copies may be obtained from the Defense Technical Information Center (DTIC) (http://www.dtic.mil).

AFRL-RV-PS-TR-2019-0009 HAS BEEN REVIEWED AND IS APPROVED FOR PUBLICATION IN ACCORDANCE WITH ASSIGNED DISTRIBUTION STATEMENT.

//signed//
ELIZABETH STEENBERGEN
Program Manager

//signed//
DAVID CARDIMONA
Tech Advisor, Missile Warning & ISR Technology Branch

//signed//
JOHN BEAUCHEMIN
Chief Engineer, Spacecraft Technology Division
Space Vehicles Directorate

This report is published in the interest of scientific and technical information exchange, and its publication does not constitute the Government's approval or disapproval of its ideas or findings.

REPORT DOCUMENTATION PAGE

Form Approved
OMB No. 0704-0188

1. REPORT DATE *(DD-MM-YYYY)*	**2. REPORT TYPE**	**3. DATES COVERED** *(From - To)*
01-04-2019	Final Report	1 Aug 2018 – 1 Apr 2019

4. TITLE AND SUBTITLE
Optical Spectroscopy of Infrared Detector Materials under Hydrostatic Pressure

5a. CONTRACT NUMBER

5b. GRANT NUMBER
FA9453-18-2-0046

5c. PROGRAM ELEMENT NUMBER
62212F

6. AUTHOR(S)
Stefan Zollner

5d. PROJECT NUMBER
6220

5e. TASK NUMBER
PPM00175356

5f. WORK UNIT NUMBER
EF131534

7. PERFORMING ORGANIZATION NAME(S) AND ADDRESS(ES) AND ADDRESS(ES)
New Mexico State University
Office of Sponsored Programs
1050 Stewart St., Ste E1200
Las Cruces, NM 88003

8. PERFORMING ORGANIZATION REPORT NUMBER

9. SPONSORING / MONITORING AGENCY NAME(S) AND ADDRESS(ES)
Air Force Research Laboratory
Space Vehicles Directorate
3550 Aberdeen Ave., SE
Kirtland AFB, NM 87117-5776

10. SPONSOR/MONITOR'S ACRONYM(S)
AFRL/RVSU

11. SPONSOR/MONITOR'S REPORT NUMBER(S)
AFRL-RV-PS-TR-2019-0009

12. DISTRIBUTION / AVAILABILITY STATEMENT
Approved for public release; distribution is unlimited.

13. SUPPLEMENTARY NOTES

14. ABSTRACT
The PI collaborated with the Air Force Research Laboratory's personnel at Kirtland Air Force Base in Albuquerque, NM, with the goal of measuring the long wavelength vibrational frequencies of infrared detector materials (germanium and germanium-tin alloys, group III/V compounds and alloys) under hydrostatic pressure in a diamond anvil cell. Progress towards this goal is described in this report.

15. SUBJECT TERMS
Raman Scattering, High Pressure, Diamond Anvil Cell, Semiconductors, Infrared Materials

16. SECURITY CLASSIFICATION OF:			**17. LIMITATION OF ABSTRACT**	**18. NUMBER OF PAGES**	**19a. NAME OF RESPONSIBLE PERSON**
					Elizabeth Steenbergen
a. REPORT	**b. ABSTRACT**	**c. THIS PAGE**			**19b. TELEPHONE NUMBER** *(include area code)*
Unclassified	Unclassified	Unclassified	SAR	24	

Standard Form 298 (Rev. 8-98)
Prescribed by ANSI Std. 239.18

(This page intentionally left blank)

TABLE OF CONTENTS

Section **Page**

LIST OF FIGURES

Figure **Page**

ACKNOWLEDGMENTS

The Principal Investigator (PI) is grateful to Dr. Elizabeth Steenbergen at the Air Force Research Laboratory (AFRL), Space Vehicles Directorate, and her group for hosting and collaborating with the PI at Kirtland Air Force Base in Albuquerque, NM, where this work was performed. The PI also acknowledges helpful discussions on Raman measurements of $Ge_{1-y}Sn_y$ alloys under hydrostatic pressure in a diamond anvil cell with Dr. Mark Holtz (Texas State University, San Marcos, TX), Dr. Suchi Guha (University of Missouri, Columbia), Dr. Jose Menendez (Arizona State University), and Dr. John Grey (University of New Mexico, Albuquerque). Samples used for this study were polished by Lilian Casias. Ge-Sn alloys used for measurements were provided by Perry C. Grant.

1.0 SUMMARY

The PI spent 54 days between 27 August and 14 December 2018 at the Air Force Research Laboratory (AFRL/RV, Space Vehicles Division) in Albuquerque, NM, at Kirtland Air Force Base to collaborate with AFRL scientists. He worked a total of 312 hours on AFRL projects. The PI collaborated with AFRL personnel at Kirtland Air Force Base in Albuquerque, NM, with the goal of measuring the long wavelength vibrational frequencies of infrared detector materials (germanium and germanium-tin alloys, group III/V compounds and alloys) under hydrostatic pressure in a diamond anvil cell. Progress towards this goal is described in this report.

2.0 INTRODUCTION

Germanium-tin alloys (with about 10% tin) are of great interest to the US Air Force as mid-wave infrared detectors, because they can be integrated with Si CMOS on cheap substrates, have high absorption coefficients in the mid-infrared spectrum, and can potentially reduce the power, weight, size, and cost in infrared detector applications. Such alloys can be under hydrostatic strain due to integration constraints. The hydrostatic strain component impacts the magnitude of the absorption coefficient due to a pressure-dependent cross-over from a direct to an indirect band structure. Pressure also changes the frequency of long wavelength (small wave vector) vibrations in crystals (which can be measured using Raman spectroscopy) and thus affects the electronic transport properties (electron and hole mobility) due to modified electron-phonon coupling. As an alternative to germanium-tin alloys, group III/V compounds, alloys, and superlattices are also of interest, depending on application, spectral range, and sensitivity.

3.0 METHODS, ASSUMPTIONS, AND PROCEDURES

To achieve high hydrostatic pressure, a small piece of a semiconductor (a plate with an approximate thickness of 30-50 μm) is placed inside a round hole (400 μm diameter) of a thin metal gasket between two flat-tip (800 μm culet) pyramids made of diamond, see Figure 1. Small ruby chips are added as pressure sensors and then the hole is filled with a pressure medium, such as alcohol. The two diamonds are pressed together by a metal membrane expanded by compressed helium gas, see Figure 2. A gas membrane pressure of 25,000 kPa (250 bar) is easily sufficient to create pressures in the cell (gasket hole) in excess of 10 GPa (100 kbar), where most semiconductors change their crystal structure. (Si and Ge convert to the body-centered tetragonal β-tin structure near 10 GPa, while the same transition in GaSb and InSb already occurs at 7 and 2.1 GPa, respectively. InAs converts to the rocksalt structure at 7 GPa.) The design of the cell allows optical access with 12 mm working distance and a 52° aperture, an angle of up 26° relative to the normal (numerical aperture of 0.48).

Mounted to an adapter plate, the diamond anvil cell is placed under a Renishaw InVia Raman microscope. The Leica DM 2700M microscope has several objectives (5X, 20X, 100X), but only the 5X magnification standard visible achromat infinity-corrected objective (Leica 506302, NA 0.12) has a sufficiently long working distance (14 mm) to allow focusing on the sample inside the diamond anvil cell. The Olympus SLMPLN20X objective (20X magnification, NA 0.25, 25 mm working distance) needs an adapter to fit on the Leica microscope, which is not yet available. The Olympus VIS SLW x50 (50X magnification, NA

0.35, 15 mm working distance) would be even better. With the 5X objective, the laser (in point focus) can be focused onto a spot of about 20 μm, much smaller than the gasket hole, see Figure 3 (The gasket hole can be Seen in the Center, with Ruby Chips Inside. The Faceted Bright to Dark Transitions show the Edge of the Diamond). Two lasers (532 nm and 785 nm emission wavelength) are available for excitation, but the 785 nm laser leads to a strong photoluminescence background that overpowers the Ge Raman signal. (The Ge band gap is 0.66 eV or 1880 nm at room temperature. Photoluminescence at twice this energy, or 940 nm and below, overlaps with the Raman signal, either because of biexciton recombination or due to detection of fundamental bandgap recombination in the second order of the diffraction grating.) Typical measurements are performed with 1% of the nominal 500 mW output power of the 532 nm continuous-wave (CW) diode-pumped solid-state laser for 100 s. Use class 3B laser safety procedures.

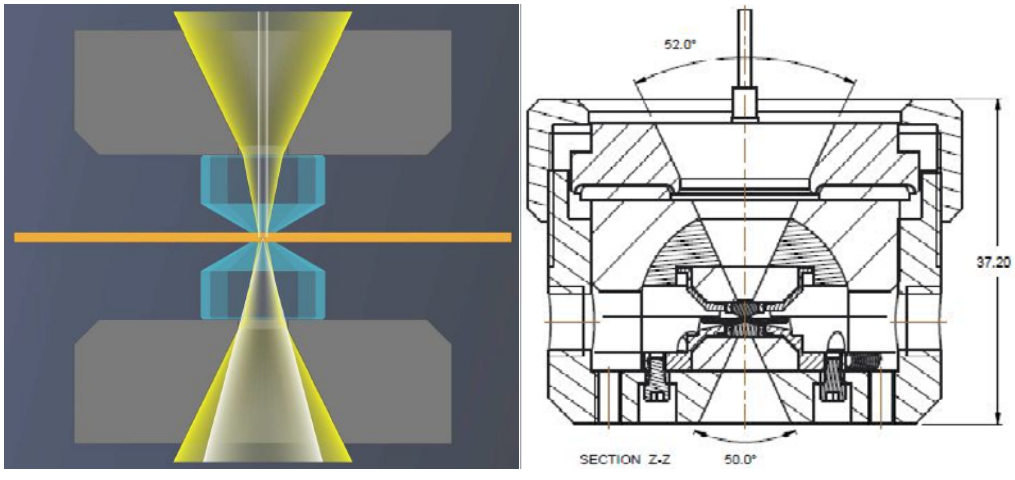

Figure 1. Left: Diamond-anvil cell Cross-section, Right: OmniDAC-LT Cross-section (Technical Drawing)

Figure 2. Left: Complete OmniDAC-LT diamond anvil cell assembly. Right: Components of the OmniDAC-LT, including (from left) DAC cylinder, piston, pressure ring, gas membrane with coiled gas line and quick connect, screw ring

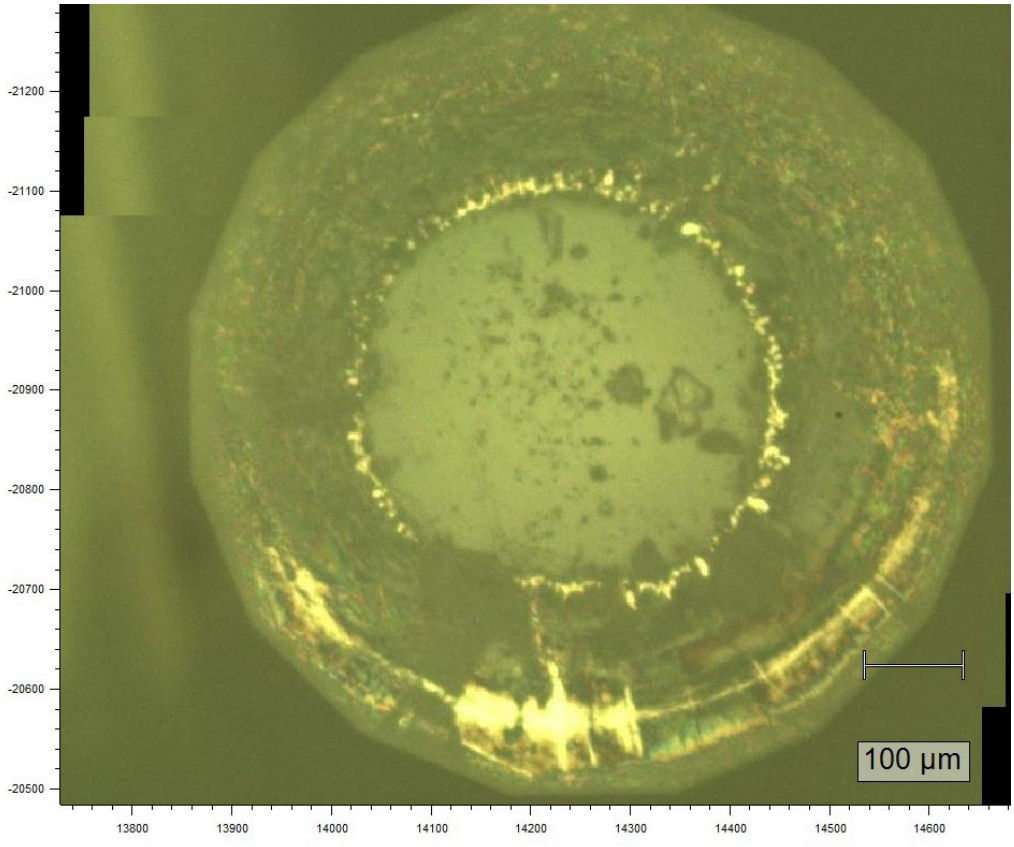

Figure 3. A View of the Metal Gasket in the Diamond Anvil Cell through the 5X Objective.

3.1 Measurement Procedure

The instrument is typically turned on in the following order: Renishaw spectrometer, computer and Wire software, laser(s). The CCD detector needs to cool down, which takes 20 minutes. Room lights need to be turned off (or the microscope enshrouded with a black cloth) to eliminate white-light and fluorescence lighting background. A suitable measurement program (such as “Si Raman calibration sample 532.wxm” or “ruby 1s.wxm”) is loaded from the “Documents” folder and executed. Spectra are stored in a proprietary format in the same directory. The Wire software can be installed on other computers to view and analyze data or export data to text. Typically, the Si Raman calibration sample will be measured initially to confirm proper operation of the instrument. If the laser spot is not inside the box (in the Wire software viewer), then an automatic alignment can be performed Tools/Alignment/Auto Align; Laser/CCD/slits). The rows on the CCD can be restricted to those illuminated by the scattered beam. A typical Si Raman spectrum is shown in Figure 4 (The background without sample is shown in red. The elastically (Rayleigh) scattered light appears near 0, the Si optical phonon at 518.3 cm^{-1}, with a width of 3.5 cm^{-1}. The second-order Si Raman spectrum can be seen below 1000 cm^{-1}. The background is constant at about 20 counts. The edge filter cuts off below 100 cm^{-1}). Typical data acquisition times are 100 s for Raman spectra and 1 s for ruby fluorescence

spectra. The typical Si Raman phonon energy is 520.8 cm^{-1}, but this depends on Si temperature, laser power, stress, doping, as well as experimental factors, such as a drift in the solid-state laser line. Due to geometric effects and scattering from optics in the spectrometer, the Rayleigh light may not be exactly at zero. Peak widths and energies are determined by line shape fitting in the Wire software.

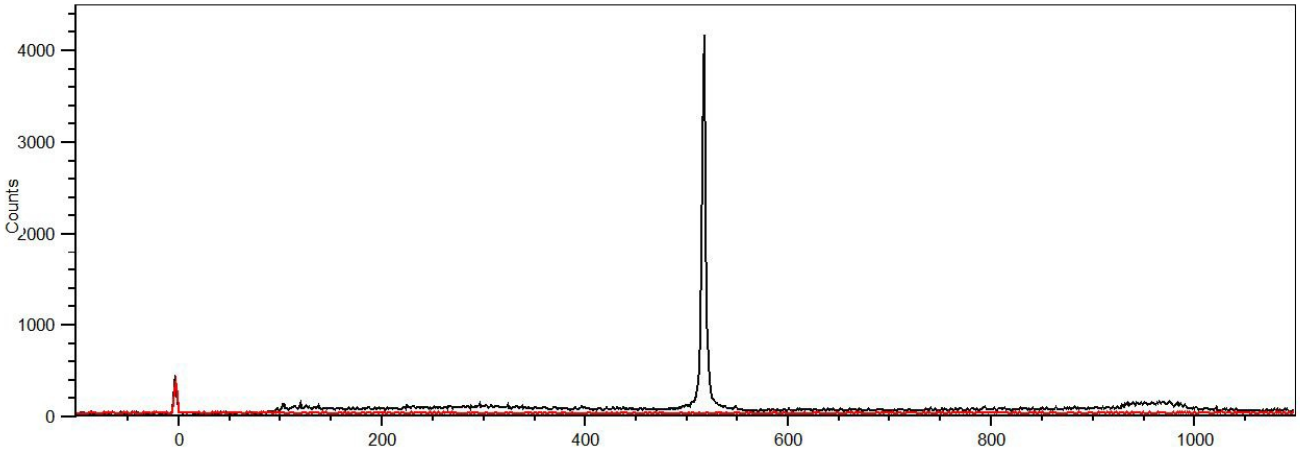

Figure 4. Typical Si Raman spectrum (black) from Renishaw calibration sample (counts versus Raman shift in cm^{-1}), measured with 5 mW (1% of 500 mW) of 532 nm laser light, integrated for 100 s.

3.2 Spectrometer Calibration

The calibration of the grating can be improved in comparison with the Renishaw Ne calibration source placed under the 5X objective by running Tools/Calibration/ Full calibration, then fitting the relevant spectrometer parameters and saving them to the registry. See separate instructions from Renishaw (inVia calibration.pdf). The S1000_2400.lns file containing the Ne line positions was modified to cover the complete spectral range from 13500 to 19000 cm^{-1}. Neutral-density filters may be needed to decrease the intensity of the Ne source.

Results are shown in Figure 5 (Orange data points show the initial calibration after the installation, red data the new calibration (both taken with an extended SyncroScan), and yellow data the energies obtained from an extended step-scan [which is best]). While there is good linearity overall (left), errors on the order of 3-5 cm^{-1} were found (right) with the extended SynchroScan. The calibration is much better for the 1200 l/mm grating than for the 2400 l/mm grating. For the 1200 l/mm grating, the average error is about zero and the maximum error about 1 cm^{-1} (with an extended SynchroScan). The errors are much larger with the 2400 l/mm grating. Initially (after installation), the errors were never zero and varied from -2.5 to -4.5 cm^{-1}. After performing a full calibration with the Ne lamp, fitting the calibration parameters and saving them to the registry, the errors were nearly zero at the highest energy, but still up to 3 cm^{-1} at lower energies. Good results (errors below 1 cm^{-1}) could only be obtained by performing extended step-scan (not SynchroScan) measurements. This needs to be taken into account when performing luminescence measurements over a broad spectral range. An extended SynchroScan is never recommended. Use the extended step-scan instead.

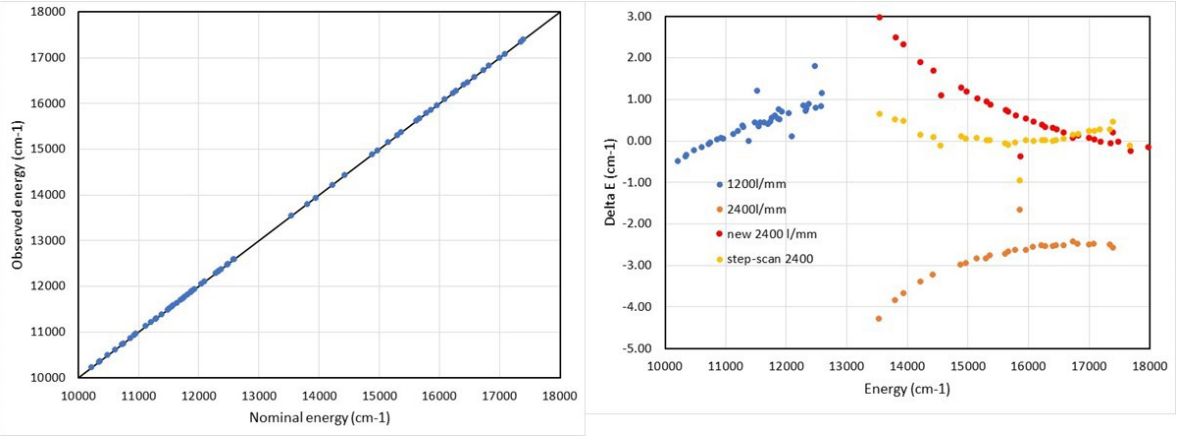

Figure 5. Calibration check of Renishaw spectrometer with Ne calibration lamp. (Left) Observed energy of the Ne gas lines versus database values in lines.txt for both gratings. (Right) Difference between observed and nominal Ne gas line energies for 1200 l/mm grating (blue) and the 2400 l/mm grating (red, yellow, orange).

3.3 Pressure Measurement with Ruby Fluorescence

The hydrostatic pressure inside the diamond anvil cell can be calculated from the Cr3+ fluorescence energy of small ruby (aluminum oxide, i.e., sapphire, doped with about 1% chromium) chips placed with the sample inside the hole of the metal gasket. The ruby emission lines can be acquired with a static measurement, where the accuracy and precision are about 0.2 cm-1, limited by the resolution of the Renishaw spectrometer. See Figure 6 for an example. The fluorescence is fitted to a double-Lorentzian with a linear (in energy) background (Ragan 1992). The older literature [2-3] used the peak maximum to represent the energy of the R1 line. The pressure can be calculated from the emission energy ν of the R1 line with the equation [3]

$$P\ [\mathrm{GPa}] = 248.4\ [(\nu_0/\nu)7.665\text{-}1] \qquad (1)$$

where ν_0 is the emission energy at zero pressure, about 14403 cm^{-1}. The exact values of the empirical parameters in Eq. (1) vary in the literature, but this is only important at pressures much larger than those of interest here. Small variations of ν_0 of about 1 cm^{-1} from chip to chip are due to variations in Cr concentration and internal strain [4]. The ruby fluorescence energies also depend on temperature [3], but the temperature and pressure dependence is usually considered to be uncoupled. For accurate pressure measurements, the temperature must be controlled to better than 1 K. When achieving a pressure of 10 GPa (100 kbar), ν will redshift by about 74 cm^{-1}, see Figure 6. A spectroscopic precision of 0.2 cm^{-1} therefore is equivalent to a pressure precision of 0.03 GPa (0.3 kbar).

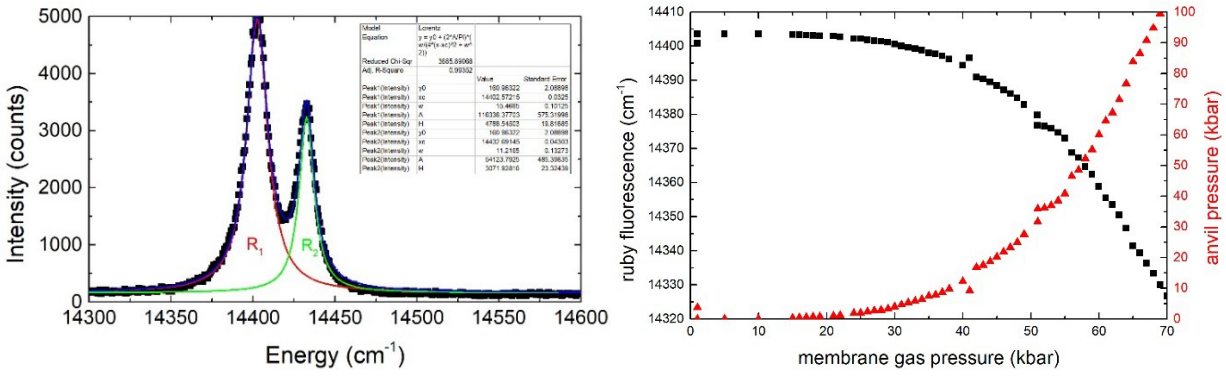

Figure 6. (Left) Fluorescence spectrum of ruby chips inside a diamond anvil cell (300 K, 1 atm) (symbols) fitted with a double-Lorentzian (no background subtracted). Red and green lines indicate the Lorentzian line shapes of the R1 and R2 lines (and the blue line their sum). (Right) R1 emission energy versus gas membrane pressure and anvil pressure calculated from Equation (1)

3.4 Raman Spectroscopy and Selection Rules

In the diamond (C, Si, Ge, Sn) or zincblende (GaAs, etc) crystal structure, the two atoms in the primitive unit cell can be excited to perform out-of-phase (optical) vibrations. For long- wavelength (small wave vector) vibrational waves (phonons), the vibrations will have the same displacement in every unit cell. Such vibrations can be observed with Raman spectroscopy, an inelastic light scattering technique, where the energies of the incident and scattered photon differ by the energy of the lattice vibration (phonon). For transverse (TO) and longitudinal (LO) optical phonons, the displacements of the atoms are perpendicular and parallel to the small wave vector of the phonon, respectively. In compound (zincblende) semiconductors, the LO phonon has a higher energy than the TO phonon, while they are the same in diamond semiconductors (and therefore labeled as LTO phonons). The TO phonons in zincblende semiconductors result in a time-varying dipole moment and therefore can also be detected with infrared absorption, reflection, or ellipsometry techniques. Not every phonon mode (LO or TO) can be observed in every Raman experiment. There are selection rules, [5-6] which depend on the geometry of the experiment, the surface orientation of the sample, and the polarization directions of the incident and scattered electric fields, see Table 1.

If a semiconductor wafer with (100) surface orientation is placed under the Renishaw microscope in backscattering geometry, then the incident and scattered light will be approximately anti-parallel, at least inside the wafer, where the refractive index is large. In the Porto notation i(j,k)l, this geometry can be written as x(j,k)-x, where j and k are the directions of the incident and scattered electric fields and the x-axis is chosen to be the surface normal. Arbitrary incident and scattered electric field vectors can be written as a superposition of fields polarized along the (001) and (011) directions and therefore we only discuss these cases. For incident light polarized along (001), there is no Raman signal, if the scattered light is also polarized along (001). Only if the incident and scattered light have orthogonal polarizations can the LO phonon be observed. This statement is reversed if the incident light is polarized along (011), when only the parallel scattering geometry is allowed. The TO phonon can never be observed in backscattering from a (100) surface, see Table 1.

Table 1. Selection rules for TO and LO phonons in Raman backscattering of zincblende semiconductors with Porto scattering notation.[6] The selection rules for diamond semiconductors are the same, except that TO and LO energies are equal.

Scattering geometry	Selection rule	
	TO phonon	LO phonon
$x(y,y)\bar{x}$; $x(z,z)\bar{x}$	0	0
$x(y,z)\bar{x}$; $x(z,y)\bar{x}$	0	$\lvert d_{\mathrm{LO}}\rvert^2$
$x(y',z')\bar{x}$; $x(z',y')\bar{x}$	0	0
$x(y',y')\bar{x}$; $x(z',z')\bar{x}$	0	$\lvert d_{\mathrm{LO}}\rvert^2$
$y'(x,x)\bar{y}'$	0	0
$y'(z',x)\bar{y}'$	$\lvert d_{\mathrm{TO}}\rvert^2$	0
$y'(z',z')\bar{y}'$	$\lvert d_{\mathrm{TO}}\rvert^2$	0
$x''(z'',z'')\bar{x}''$	$(2/3)\lvert d_{\mathrm{TO}}\rvert^2$	$(1/3)\lvert d_{\mathrm{LO}}\rvert^2$
$x''(z'',y'')\bar{x}''$	$(2/3)\lvert d_{\mathrm{TO}}\rvert^2$	0

When the sample is placed inside the gasket hole of the diamond anvil cell, the (100) surface of the sample might not be perpendicular to the beam and therefore the backscattering selection rules shown in Table I might not be satisfied. Also, scattering might occur not only from the (100) surface of the sample, but also from the cleavage planes, i.e., the (110) surface for zincblende semiconductors and the (111) surface for diamond semiconductors. [7] This would explain why one might observe not only the LO, but also the TO phonon inside the diamond anvil cell. Hydrostatic pressure does not change the symmetry of the crystal and therefore the selection rules in Table 1 are still valid.

In doped semiconductors, the TO phonon is not affected, but the free carriers will interact with LO phonons to form lower (LPP) and upper (UPP) phonon-plasmon polaritons [8-9]. These polaritons are much broader and often have lower scattering cross-sections than the sharp LO Raman peaks in undoped semiconductors. Also, at very high carrier concentrations, the electron/hole plasma screens the Fröhlich interaction (LO/TO splitting) and therefore the LPP mode approaches the energy of the TO mode for high doping. Such polaritons are typically studied in a right-angle geometry with a laser energy below the bandgap, since a 532 nm laser in backscattering might not penetrate the surface depletion region and therefore might not probe the heavily doped volume.

4.0 RESULTS AND DISCUSSION

4.1 Raman Spectroscopy Examples

Figure 7 shows examples of Raman spectra obtained with the 5X objective of the Renishaw microscope on various (100) semiconductor surfaces. Only LO phonons are observed on (100) surfaces, see Table 1. In our experimental configuration, neither the incident nor scattered polarization are known, since no polarizers are inserted in the beam path. The incident laser is polarized (100:1 vertical), but this might be affected by the beam steering inside the spectrometer. The scattered light is affected by the spectrometer throughput function (especially the diffraction grating), which usually favors one polarization. Given these polarization conditions and the selection rules, the scattering intensity will normally change when rotating the wafer by 45°, but this is difficult to quantify without an actual polarizer in the beam path. There are systematic changes in the phonon energy across various zincblende materials. To first order, the phonon energy is inversely proportional to the square root of the reduced mass of the two atoms in the unit cell.

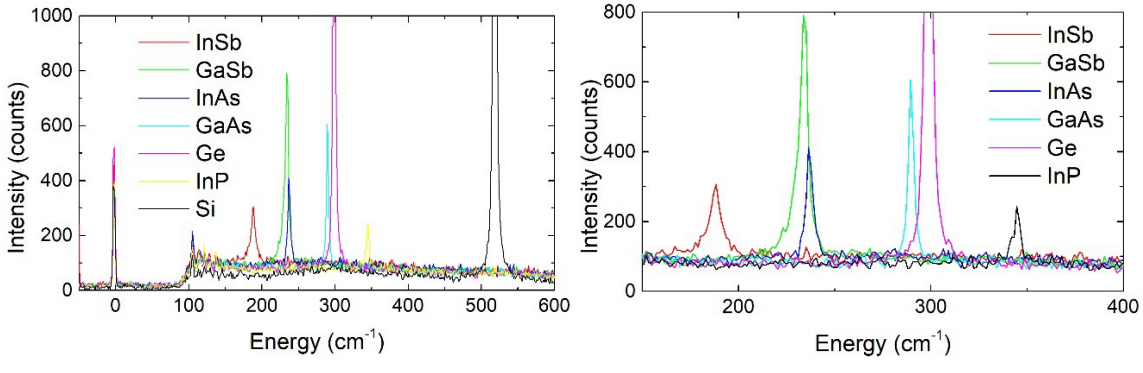

Figure 7. Raman spectra for different semiconductor (100) surfaces in backscattering geometry, acquired with the 532 nm laser (5 mW, 100 s integration). The plot on the right is zoomed in

4.2 Alloy Phonons

In a binary group-IV semiconductor alloy, we will observe not only one phonon mode (as in the element), but three, for example Sn-Sn, Ge-Ge, and Ge-Sn modes in $Ge_{1-y}Sn_y$ alloys, which have intensities proportional to y^2, $(1-y)^2$, and $y(1-y)$, respectively. For Sn contents below 20%, only the Ge-Ge mode was observed in our alloys using the Renishaw spectrometer. (Perhaps

better background suppression and longer integration would also show the other modes.) The Ge-Ge and Sn-Sn modes in the $Ge_{1-y}Sn_y$ alloy have approximately the same energy as in the element, but there are small corrections due to alloy content. The energy of the Ge-Ge mode in unstrained $Ge_{1-y}Sn_y$ alloys is given by

$$\omega(y)= \omega(Ge)-\alpha y \quad (2)$$

where α=75 cm^{-1} [10]. Figure 8 (For several samples, the Ge-Ge vibration is significantly higher than expected, most likely due to residual strain**)** shows Raman spectra for several $Ge_{1-y}Sn_y$ alloys (grown on a Ge buffer layer on a Si substrate). In general, the Ge-Ge Raman peak redshifts with increasing tin content and loses intensity for completely relaxed alloys, but strain is also a factor, especially if the alloy layer is thinner than the critical thickness.

4.3 Strain Correction

A tetragonal distortion of the $Ge_{1-y}Sn_y$ alloy layer due to a biaxial in-plane stress for growth on a (001) surface will split the triply-degenerate zone-center LTO phonons into a singlet (vibrations along the surface normal) and a doublet (vibrations in the plane). In the standard backscattering geometry from a (001) surface, only the singlet is observable. [11] It has an energy

$$\omega(\varepsilon_{\parallel})=\omega_0+b\varepsilon_{\parallel} \quad (3)$$

where $\varepsilon\parallel$ is the in-plane strain, $\omega 0$ the energy of the vibration of the phonon in the unstrained alloy, and b the phonon deformation potential. For the Ge-Ge mode in $Ge_{1-y}Sn_y$ alloys, we choose b=–415 cm^{-1}, the same value as in bulk Ge. [10]

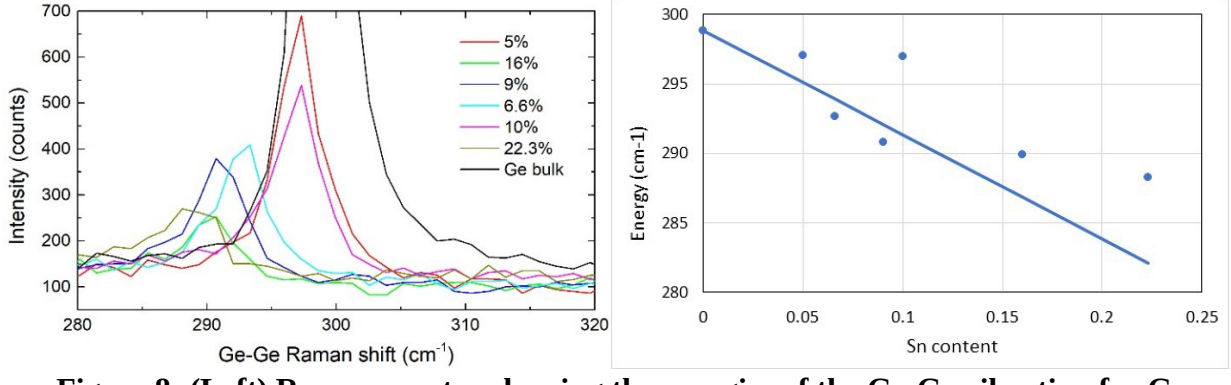

Figure 8: (Left) Raman spectra showing the energies of the Ge-Ge vibration for $Ge_{1-y}Sn_y$ alloys with varying composition in comparison with bulk Ge (samples from a commercial equipment manufacturer). (Right) Measured peak positions versus tin content (symbols) in comparison with the theory (line) given in Equation (2) for completely relaxed alloys.

4.4 Lineshape of Raman peaks in $Ge_{1-y}Sn_y$ alloys

The Raman lines in semiconductor alloys are asymmetric and cannot be described using the symmetric peak line shapes implemented in the Renishaw Wire software. Lockwood and Walisewski [12] recommend a line shape of the form

$$I_{\mathrm{EMG}}(\omega) = \frac{a}{2s}\exp\left(\frac{w^2}{2s^2} + \frac{\omega_0-\omega}{s}\right)\left[\mathrm{erf}\left(\frac{\omega-\omega_0}{\sqrt{2}w} - \frac{w}{\sqrt{2}s}\right) + \frac{s}{|s|}\right] \quad (4)$$

for $Al_xGa_{1-x}As$ alloys. This has also been adopted for $Ge_{1-y}Sn_y$ alloys [10]. A symmetric Lorentzian is the natural phonon line shape in a pure compound. A Gaussian is the line shape of an infinitely sharp line limited by resolution. A symmetric Gaussian-Lorentzian therefore works well for optical phonons in compound semiconductors, but not for alloys. In addition to the Raman line (4) itself, one needs a background function, which is usually taken as [10]

$$I_{\mathrm{back}}(\omega)=b_1+b_2\omega^{-m}. \quad (5)$$

Since Eq. (4) is not implemented in the Renishaw Wire software, one needs to export the Raman data into a text file, which can then be imported into Igor Pro or Origin and fitted there. We note that the parameter *s* is negative for a Raman line broadened asymmetrically towards lower energies, as in our case.

Figure 9 shows an example of such a fit for a $Ge_{1-y}Sn_y$ alloy with y=16%. The background here is about 100 counts and the signal is 150 counts. Renishaw has been asked about the origin of this high background, but no answer has been received yet. (The background in the spectra is much lower with the laser off, so the background is not due to the dark current in the CCD detector.) Due to the low spectral resolution of the Renishaw instrument (even with a 2400 lines/mm grating), there are only about 10 data points across the Raman peak for this sample. It appears that the line is asymmetric, with a slow rise (at low energies) and a rapid drop at high energies. This asymmetry can be described well with Eq. (4), but not with Gaussian or Lorentzian line shapes.

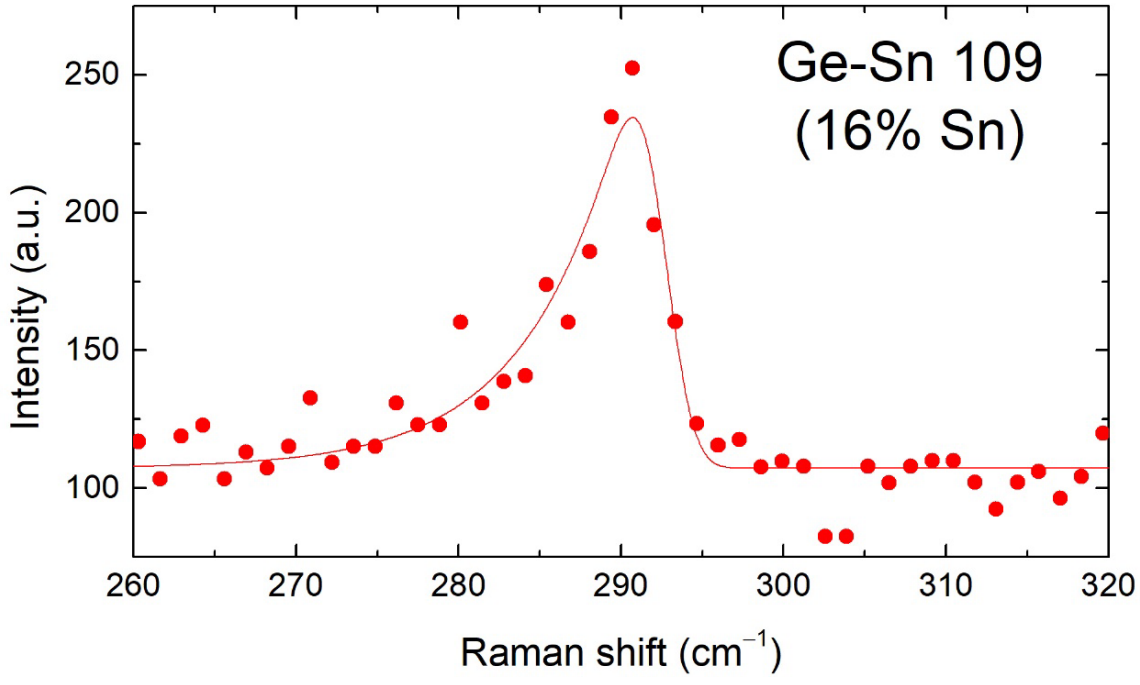

Figure 9. Raman spectrum for a Ge-Sn alloy with 16% Sn (symbols) in comparison with the best fit to the asymmetric line shape in Equation (4) with a linear background

4.5 Raman Measurements in the Diamond-Anvil Cell

An attempt was made to measure Raman spectra of a Ge plate inside the diamond anvil cell, but only a weak signal and a high background were found, see Figure 10 (The peak near 300 cm^{-1} is very weak and the background is high. The blue line shows the Raman spectrum when the laser is focused on a ruby chip. The Ge Raman signal disappears, but the background is nearly unchanged. The red line shows the spectrum when the laser only hits the Nujol pressure medium (heavy paraffin oil). We conclude that the background does not arise from the ruby chips or from the Nujol, but from the diamonds, which are not optimized for low-background Raman measurements). The diamonds used for these experiments were synthetic type IIac diamonds. Type IIa indicates that these diamonds have very little infrared absorption due to a low nitrogen impurity content. The last letter “c” indicates that the diamonds were produced by chemical vapor deposition. Such diamonds are not ideal for Raman spectroscopy due to a moderately low fluorescence background with 532 nm laser excitation. Instead, diamonds of type IIas are required for Raman spectroscopy, due to their ultra-low fluorescence background and ultra-low birefringence. The pressure dependence of the Raman phonons in Ge was measured by Olego and Cardona. [13]

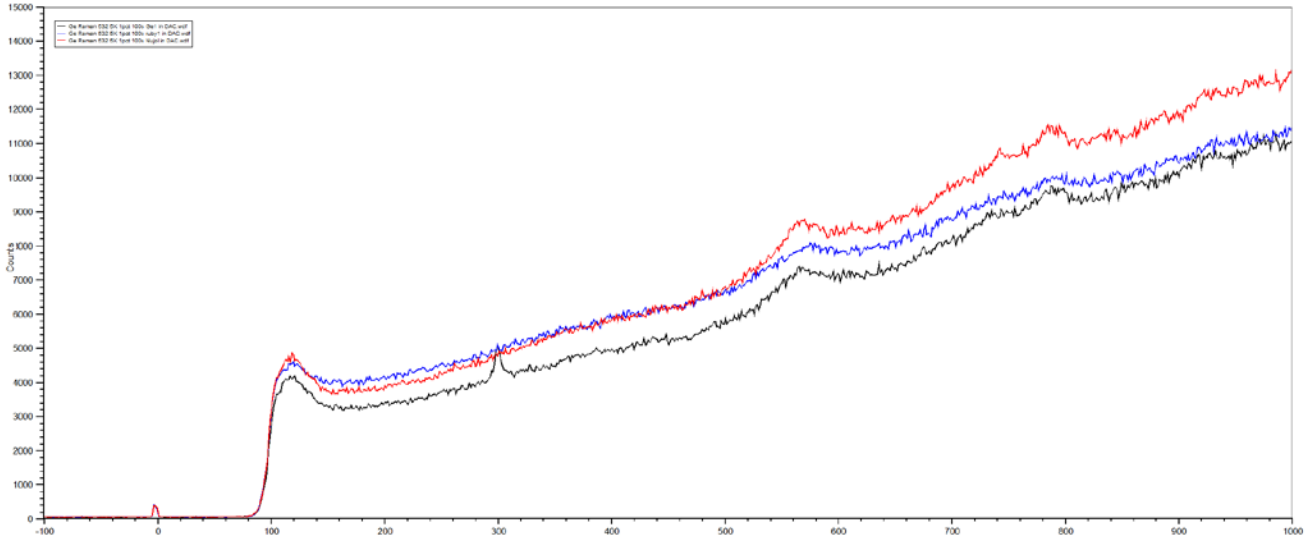

Figure 10. Raman shift (as a function of wave number) for a Ge plate inside the diamond anvil cell at atmospheric pressure (black).

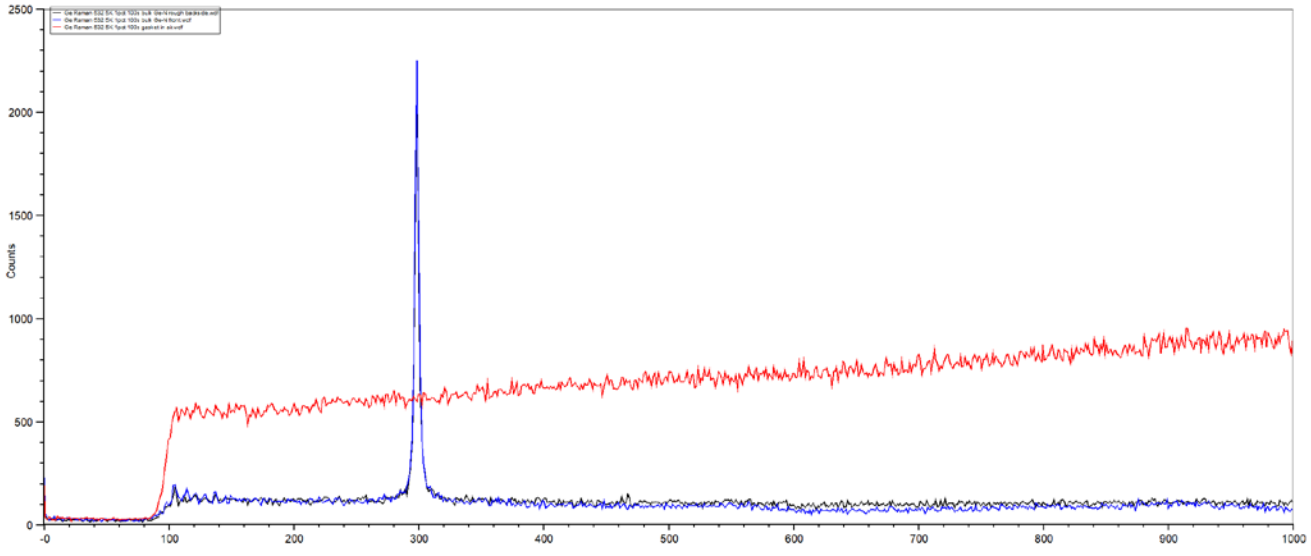

Figure 11. Raman shift of Ge in air from the polished front (blue) and rough back (black) surfaces of a thinned Ge plate with 100 µm thickness. Both are nearly the same, so the Raleigh scattering from the rough back surface is not an issue. The red line shows the Raman spectrum when the laser is focused on the Cu-Be gasket. It shows a broad background, but not the characteristic diamond-related peaks seen in Figure 10

5.0 CONCLUSIONS

The PI collaborated with AFRL personnel at Kirtland Air Force Base in Albuquerque, NM, with the goal of measuring the long wavelength vibrational frequencies of infrared detector materials (germanium and germanium-tin alloys, group III/V compounds and alloys) under hydrostatic pressure in a diamond anvil cell. Progress towards this goal is described in this report.

REFERENCES

[1] G. J. Piermarini, S. Block, J. D. Barnett, and R. A. Forman, "Calibration of the pressure dependence of the R1 ruby fluorescence line to 195 kbar," *Journal Applied Physics*, vol **46**, 1975, pp. 2774-2780.

[2] H. K. Mao, P. M. Bell, J. W. Shaner, and D. J. Steinberg, "Specific volume measurements of Cu, Mo, Pd, and Ag and calibration of the ruby R1 fluorescence pressure gauge from 0.06 to 1 Mbar," *Journal Applied Physics*, vol **49**, 1978, pp. 3276-3283.

[3] R. Goñi and K. Syassen, "Optical properties of semiconductors under pressure," *Semiconductors and Semimetals*, vol **54**, 1998, pp. 247-425.

[4] I. De Wolf, "Micro-Raman spectroscopy to study local mechanical stress in silicon integrated circuits," *Semiconductors. Science and Technology*, vol **11**, 1996, pp. 139-154.

[5] D. D. Ragan, R. Gustavsen, and D. Schiferl, "Calibration of the ruby R1 and R2 fluorescence shifts as a function of temperature from 0 to 600 K," *Journal Applied Physics***,** vol **72**, 1992, pp. 5539-5544.

[6] P. Y. Yu and M. Cardona, **Fundamentals of Semiconductors,** Springer Publishing, Berlin, Germany, 2010.

[7] R. Peréz and P. Gumbsch, "An ab initio study of the cleavage anisotropy in silicon," *Acta Materialia*, vol **48**, 2000, pp. 4517-4530.

[8] A. Mooradian and G. B. Wright, "Observation of the interaction of plasmons with longitudinal optical phonons in GaAs," *Physical Review Letters*, vol **16**, 1966, pp. 999-1001.

[9] A. Mooradian and A. L. McWhorter, "Polarization and intensity of Raman scattering from plasmons and phonons in gallium arsenide," *Physical Review Letters*, vol **19**, 1967, pp. 849-852.

[10] V. R. D'Costa, J. Tolle, R. Roucka, C. D. Poweleite, J. Kouvetakis, and J. Menéndez, "Raman scattering in Ge1-ySny alloys," *Solid State Communications*, vol **144**, 2007, pp. 240-244.

[11] S. Ganesan, A. A. Maradudin, and J. Oitmaa, "A lattice theory of morphic effects in crystals of the diamond structure," *Annals of Physics*, vol **56**, 1970, pp. 556-594.

[12] D. J. Lockwood and Z. R. Wasilewski, "Optical phonons in AlxGa1-xAs: Raman spectroscopy," *Physical Review B*, vol **70**, 2004, p. 155202.

[13] D. Olego and M. Cardona, "Pressure dependence of Raman phonons of Ge and 3C-SiC," *Physical Review B*, vol **25**, 1982, p. 1151.

DISTRIBUTION LIST

DTIC/OCP
8725 John J. Kingman Rd, Suite
0944 Ft Belvoir, VA 22060-6218 1 cy

AFRL/RVIL
Kirtland AFB, NM 87117-5776 1 cy

Official Record Copy
AFRL/RVSU/Elizabeth Steenbergen 1 cy

(This page intentionally left blank)